

Variable-spot ion beam figuring

Lixiang Wu^{a,*}, Keqiang Qiu^a, Shaojun Fu^a

^a*National Synchrotron Radiation Laboratory, University of Science and Technology of China, Hefei 230029, China*

Abstract

This paper introduces a new scheme of ion beam figuring (IBF), or rather variable-spot IBF, which is conducted at a constant scanning velocity with variable-spot ion beam collimated by a variable diaphragm. It aims at improving the reachability and adaptation of the figuring process within the limits of machine dynamics by varying the ion beam spot size instead of the scanning velocity. In contrast to the dwell time algorithm in the conventional IBF, the variable-spot IBF adopts a new algorithm based on the scan path programming and the trajectory optimization using pattern search. In this algorithm, instead of the dwell time, a new concept, integral etching time, is proposed to interpret the process of variable-spot IBF. We conducted simulations to verify its feasibility and practicality. The simulation results indicate the variable-spot IBF is a promising alternative to the conventional approach.

Keywords: Ion beam figuring, Removal function, Trajectory optimization, Integral etching time, Spatio-temporal visualization

1. Introduction

IBF is a powerful technique for enabling ultra-precision finishing of optical surfaces [1, 2]. As a deterministic method, it has proven effective and applicable in processing both large optics [3, 4] and small optical components [5]. For

*Corresponding author

Email addresses: wulx@mail.ustc.edu.cn (Lixiang Wu), blueleaf@ustc.edu.cn (Keqiang Qiu), sjfu@ustc.edu.cn (Shaojun Fu)

years, it has seen a growing demand of the high-quality ultra-precision optics finished by IBF technologies in many fields such as astronomy telescopes [3, 4], synchrotron beamlines [6, 7, 8], and the extreme ultraviolet lithography [9].

As is well known, the conventional figuring process can be considered as a typical convolution process, in which the controlled ion beam with fixed Gaussian-shaped profile scans over a workpiece with variable dwell velocities. Energetic ions impinge on dwell points or local areas of the workpiece surface so that materials are removed in proportion to the desired material removal. The calculation of dwell times that determine the figuring process is an ill-posed deconvolution problem meanwhile it plays a crucial role in achieving high accuracy of the IBF [10, 11]. This method can be traced back to the computer-controlled optical surfacing (CCOS), which is a breakthrough technology in the optical fabrication field [12].

We believe the conventional method is not the only scheme for IBF. And here we put forward a new scheme of IBF with some practical benefits and new concepts. Instead of varying the scanning velocity of ion beam, our method is realized by dynamically adjusting the spot size of ion beam via a variable diaphragm, which is also called variable-spot IBF. In contrast to the conventional approach, where a fixed diaphragm is usually used [13] and thus an invariant removal function is obtained, the variable-spot IBF involves a variable diaphragm that collimates the ion beam and then forms a spatially and temporally variable ion beam spot on the workpiece surface, which results in a variable-spot removal function. In addition, the variable-spot IBF would prefer to run at a constant scanning velocity. We can really benefit a lot from the two key properties of variable-spot IBF, i.e., variable spot and constant scanning velocity. First, the ion beam with variable spot has a better adaptation to the target material removal because ion beams with different spot sizes are applicable in removing surface errors of different spatial frequencies. Second, scanning at a constant speed leads to a more reliable and steady figuring process. And third, as a minor point, it is more convenient and economical to adjust the variable diaphragm than to control the scanning motion of ion source.

The variable-spot IBF is not a convolution process so that we cannot adopt the dwell time algorithm of the conventional IBF. Recently, we give a new interpretation of the process of the variable-spot figuring process based on the concept of integral etching time and the spatial-temporal analysis, and at the same time, propose an algorithm for the variable-spot IBF. The algorithm consists of two parts: scan path programming and trajectory optimization. By the scan path programming, the two-dimensional figuring is reduced into the one-dimensional figuring. Then the trajectory optimization of one-dimensional figuring using pattern search is conducted on the basis of the S-curve transformation with consideration of the limits of machine dynamics. Through the S-curve transformation, an etching time profile determined by trapezoidal velocity profiles of driving motors of the variable diaphragm is optimized to fit to the target profile. The optimization can directly generate the motion profile, which is an obvious advantage over the conventional method that requires an approximate conversion from the dwell times to dwell velocities.

2. Variable-spot ion beam

2.1. Design of variable diaphragm

We designed a variable diaphragm to dynamically collimate the ion beam emitted from a broad ion source and adjust its dimensions. As is illustrated in Figure 1, in the course of IBF, the round ion beam is collimated by the variable diaphragm with two pairs of shutters into a rectangular beam. The variable diaphragm is dragged by a linear motor and its aperture diameter $\Phi(t)$ is proportional to the translation distance $D(t)$ of the motor such that

$$\Phi(t) = kD(t), \quad (1)$$

where k is the gear ratio. Note that though the variable diaphragm contains two pairs of shutters, only one moves and another is temporarily fixed during the figuring process. So the aperture diameter $\Phi(t)$ here refers to the distance of the two moving shutters. The center of ion beam always coincides with the aperture center during the IBF process and the beam profile is symmetric.

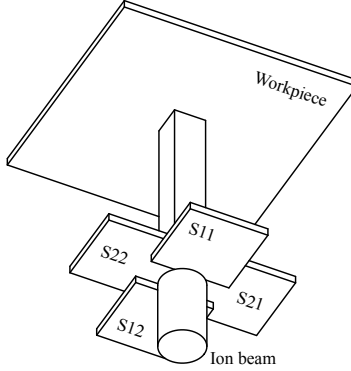


Figure 1: IBF with the variable diaphragm. Note that S11(S21) and S12(S22) is a pair of shutters, which is driven by a single linear motor.

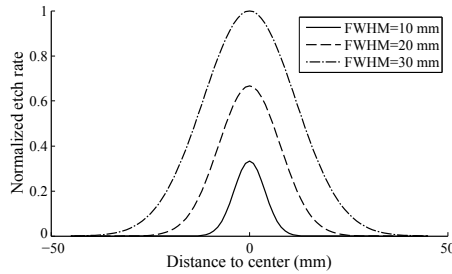


Figure 2: A family of normalized Gaussian removal functions.

2.2. Assumptions of variable-spot removal function

The Kaufman ion source is widely used in IBF [14] and it typically induces a removal function with Gaussian profile in the figuring of planar optics [15]. Figure 2 shows a family of one-dimensional normalized Gaussian removal functions with different full widths at half maximum (FWHMs), which are the results of controllable adjustments of the aperture size of the variable diaphragm. For convenience, we make an assumption that the FWHM of removal function equals to the aperture size of the variable diaphragm and the maximum of the removal function linearly decreases as the diaphragm aperture narrows.

Based on the one-dimensional removal function, the removal function with two-dimensional distribution is also generated, which is the vector multiplication

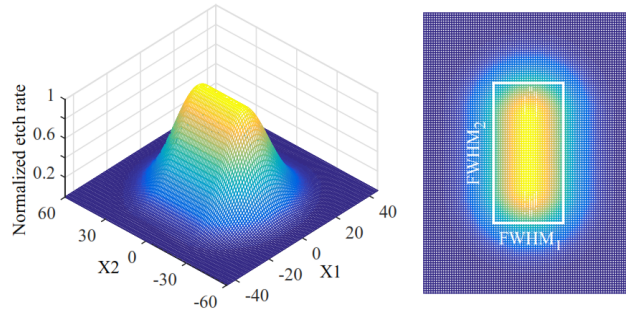


Figure 3: Removal function. The white rectangle with two sides of lengths of FWHM_1 and FWHM_2 on the right indicates the diaphragm aperture.

of two one-dimensional removal function. The details are illustrated in Figure 3, where FWHM_1 and FWHM_2 represent the full widths at half maximum of the vertical profile and the transverse profile respectively. The rectangle, of which one side has a length of FWHM_1 and another has a length of FWHM_2 , coincides with the aperture dimensions of the variable diaphragm.

2.3. Practical considerations

It is reasonable to make an assumption of variable-spot removal functions, which serves as a convenience to the simulations that demonstrate the process of variable-spot IBF and verify the feasibility of our proposed method. However, this assumption cannot be applicable in the real cases of variable-spot IBF since the removal functions should be accurately measured by experiments or the mathematical modeling based on material removal characteristics. W. Liao *et al.* studied the mathematical modeling and application of removal functions during deterministic IBF of optical surfaces [15, 16]. It suggests that mathematical models that are developed theoretically and verified experimentally can help to build the removal function database. In practice, we should also develop a database of variable-spot remove functions, which is applicable in the variable-spot IBF of optical elements.

3. Preliminary analysis

3.1. Integral etching time

Whether to adjust the aperture of ion beam during the figuring process or not is one of the most significant differences between the conventional IBF and the variable-spot IBF. The process of variable-spot IBF is not a convolution process since the removal function is time-varying due to the dynamic adjustment of beam aperture by the variable diaphragm. So we try to understand the process of variable-spot IBF on the basis of the concept of integral etching time.

The Gaussian removal function $B(x; t)$ is assumed as

$$B(x; t) = B_n(x; t)r_{etch,max}, \quad B_n(x; t) = \frac{\Phi(t)}{\Phi_0} \exp[-4 \ln 2 \left(\frac{x - s(t)}{\Phi(t)}\right)^2], \quad (2)$$

where $B_n(x; t)$ is the normalized Gaussian removal function, $r_{etch,max}$ is the maximum etch rate, $s(t)$ represents the scanning position of the beam center, $\Phi(t)$ represents the aperture diameter of the variable diaphragm and Φ_0 is the maximum aperture diameter. And the integral etching time $T_{etch}(s)$ is defined as

$$T_{etch}(s) = \int_{t=0}^{\infty} B_n(s; t) dt. \quad (3)$$

So the material removal $R(s)$ can be reinterpreted as

$$R(s) = \int_{t=0}^{\infty} B(s; t) dt = \int_{t=0}^{\infty} B_n(s; t)r_{etch,max} dt = T_{etch}(s)r_{etch,max}. \quad (4)$$

A new term, integral etching time, is introduced here to describe the integrated time weighted by the normalized removal function, which is abbreviated as etching time hereafter. As illustrated by Equations (2), (3), and (4), the integral etching time is a hub connecting the removal function with the desired material removal.

3.2. Spatio-temporal visualization of the figuring process

We present a demonstration of spatio-temporal visualization of the two different figuring processes in one-dimensional case to further explore the relationship between the variable-spot IBF and the conventional IBF. Figure 4 (a) illustrates a conventional figuring process with a time-invariant Gaussian removal

function in a spatio-temporal coordinate system, where the twisted rainbow indicates the track of the normalized Gaussian removal function. Figure 4 (b) demonstrates a typical variable-spot IBF process, which operates at a constant scanning velocity with a variable-spot ion beam.

Both cases shown in Figure 4 have an identical target material removal (the sinusoidal curves in red). The former result is calculated using the *deconvlucy* function in Matlab, which is an implementation of the Lucy-Richardson method [17]. The latter result is obtained by the trajectory optimization based on the modified fine adjustment algorithm [18]. The preliminary simulations indicate that variable-spot IBF is a possible alternative technique to the conventional IBF.

4. Algorithm for variable-spot IBF

4.1. Scan path programming

In the sub-aperture polishing, the tool path should be generated before the calculation of dwell times. Similarly, the scan path of the variable-spot ion beam should also be programmed before the trajectory optimization in the variable-spot IBF. We proposed a simple scheme for programming scan paths of the variable-spot ion beam. It consists of three steps: rastering, grouping, and superposition, which is shown in Figure 5. First, the ion beam scans boustrophedonically over the desired surface map or etch-depth map along a zig-zag track. Then, the zig-zag track is broken down into many linear paths, which are classified as several groups, and correspondingly the averaged surface maps are reduced into fringe patterns. And finally, the programmed surface map is obtained by point-to-point superposition of the fringe patterns. In the step of grouping, the linear paths that have both an identical direction and a uniform transverse distance are classified as a layer. The transverse distance of the linear paths in a layer equals to the width of the ion beam. The number of linear paths within a distance of the ion beam width should be positive even such as 2, 4, 6, and so on, which determines the number of layers in the grouping step.

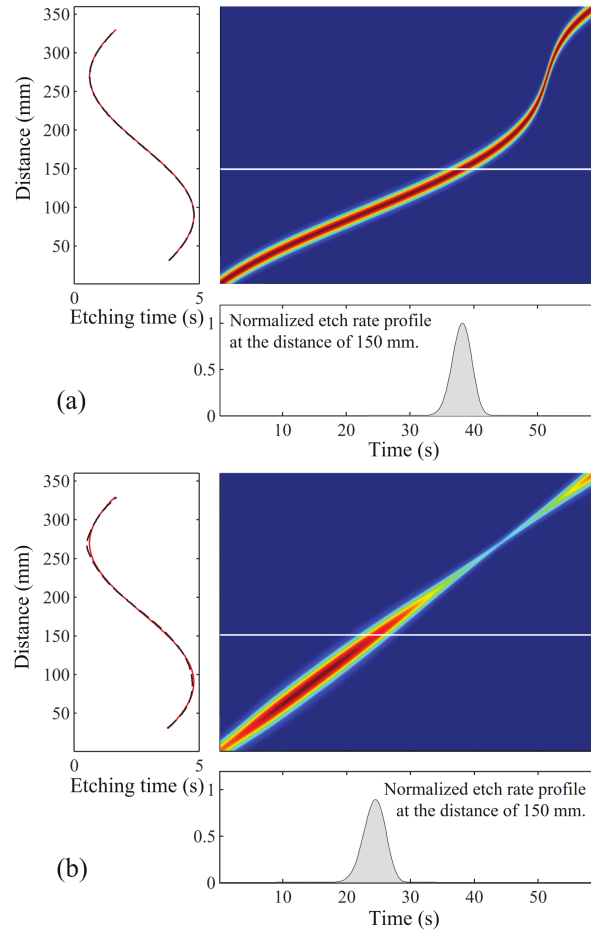


Figure 4: Spatio-temporal visualization of (a) the conventional IBF process (b) and the variable-spot IBF process. Both processes aim at fitting an identical target material removal. The sinusoidal solid curves in red indicate the material removals and the dotted curves are the calculated results.

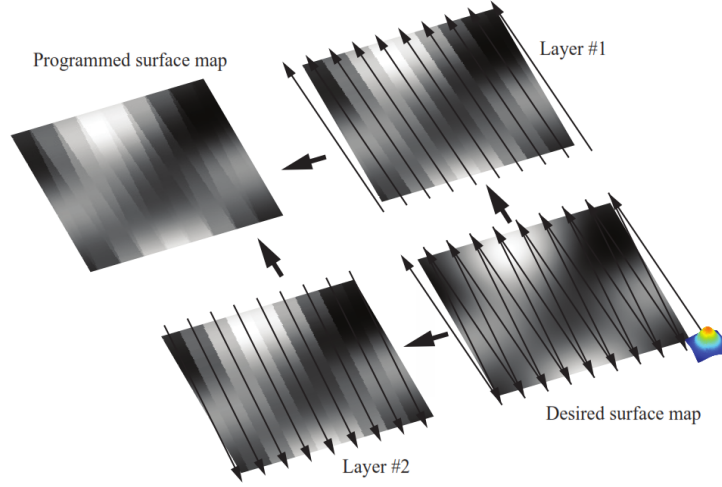


Figure 5: Illustration of scan-path programming. There are three processing steps, that are rastering, grouping, and superposing, from the desired etch-depth map to the programmed etch-depth map.

Note that after the process of scan path programming, we can horizontally rotate the workpiece to a quarter turn, then conduct the scan path programming again, and the crossing of the two times of programming will result in a more smoothing programmed map.

After the programming of scan paths, programmed etching time profiles, corresponding to profiles of the fringe patterns, are calculated according to Equation 4. The etching time profile is the ratio of the programmed etch-depth profile, i.e. the profile of fringe pattern in the programmed surface map, to the maximum etch rate. The calculated etching time profiles are shown in Figure 6.

4.2. Trajectory optimization

The trajectory optimization is based on the etching time instead of the dwell time. And the objective is to find a sequence of feasible motion trajectories of driving motors of the variable diaphragm that make the calculated etching time profiles as close as possible to the programmed etching time profiles.

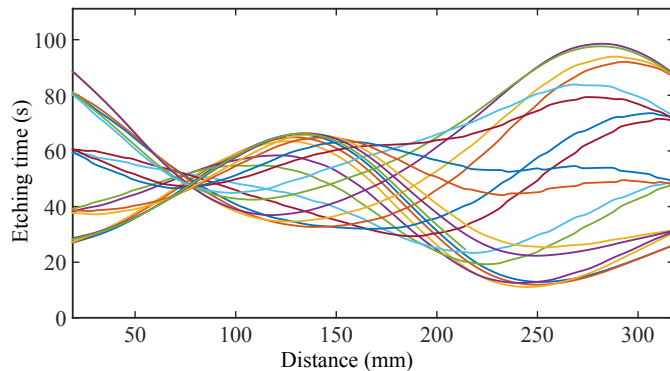


Figure 6: Programmed etching time profiles.

4.2.1. Machine dynamics

Generally, the machine dynamics would limit the reachability and determinacy of IBF. Meanwhile, finite are the limits of machine dynamics mainly including the maximum velocity and acceleration of the scanning ion beam system or the workpiece stage. In our design, the beam scanning velocity keeps constant in the course of IBF while the ion beam is collimated by the variable diaphragm so that the beam spot is dynamically adjusted.

The initial estimate of beam scanning velocity is

$$v_{scan} = r \frac{\int_{-\infty}^{\infty} B_n(x; t_0) dx}{\max(T_{etch})}, \quad (5)$$

where r is an empirical parameter with default value of 1, $\max(T_{etch})$ indicates the maximum of the target etching times.

Trapezoidal velocity profiles [19] are applied to providing smooth motion for motors of the variable diaphragm. Currently, we only use trapezoidal velocity profiles to define the motion trajectory of motors. Because the trapezoidal velocity profile is the simplest scheme for motion smoothing and the number of its control parameters is also less than the other motion profiles.

4.2.2. S-curve transformation

In our previous work [18], we first found that there exists a correspondence relationship between the trapezoidal velocity profile of the driving motor and

the S-shaped etching time profile along the scan path. The shape of an etching time profile can be adjusted by tuning control parameters of the corresponding trapezoidal velocity profile, which is the key point of S-curve transformation. Moreover, the programmed etching time profiles can be represented by B-splines [20], and theoretically a B-spline can be divided into a group of S-curves taking the stationary points as the division points. So, for a desired etching time profile, the trajectory optimization is to find a sequence of trapezoidal velocity profiles determining an etching time profile close to the desired etching time profile. The root-mean-square deviation (RMSD) of the calculated etching time profile and the desired etching time profile should be within the specified maximum deviation.

4.2.3. Trajectory optimization using pattern search

Pattern search is a family of direct-search methods without using derivatives of the problem to be optimized, which is deterministic and suitable for optimizing the problem of one-dimension variable-spot IBF. For this optimization problem, it follows the basic generalized pattern search algorithm of tree steps: initialization, search and poll steps, and parameters update [21].

The first step is to determine the initial or starting point and the objective function. The starting point, which is a vector or pattern, includes the perturbations of diaphragm diameter at the division points, the acceleration and deceleration for adjusting the trapezoidal velocity profile. The objective function is the RMSD of the calculated etching time curve and the target etching time spline. And then perform the search and possibly the poll steps. Finally, update parameters iteratively until adapting to the target. Based on the S-curve transformation, the parameters that determines the trapezoidal velocity profiles are iteratively adjusted for improving the fit to the S-shaped etching time profiles which comprise the desired etching time spline.

Table 1: Simulation parameters.

Parameter	Value	Parameter	Value
v_{scan}	0.292 mm/s	k	1/1000
v_u	200 mm/s	a_u	2 mm/s ²
Φ_0	30 mm	r	1
$N_{iter,max}$	360	$r_{etch,max}$	1 mm/s

5. Simulations and discussions

Two simulations are conducted. The first simulation example is demonstrated to detail the processes and results of the aforementioned trajectory optimization using pattern search in one-dimensional figuring. And we select one of programmed etching time profiles as the target etching time profile in this simulation. The second simulates a real world process of two-dimensional figuring and aims at verifying the feasibility of variable-spot IBF. The desired surface map is a random rough surface with Gaussian statistics generated by the RSG code [22].

5.1. Trajectory optimization of one-dimensional figuring

The simulation parameters and their values are shown in Table 1, where $N_{iter,max}$ indicates the maximum number of iterations and is specified as the stop condition.

Figure 7 shows the processing results of an iteration in the trajectory optimization. First, the target etching time spline is divided into a group of S-curves taking the stationary points as the division points (the red circles in Figure 7 (a)). And then it polls a pattern to adjust the motion profile of the variable diaphragm. The pattern is a vector containing control parameters of trapezoidal velocity profiles. The feasible regions, marked by the red dotted lines in Figure 7 (b), indicate the limits of machine dynamics of the variable diaphragm. The parameter optimization of the trapezoidal velocity profile is conducted within the feasible regions. Finally, the optimized etching time is

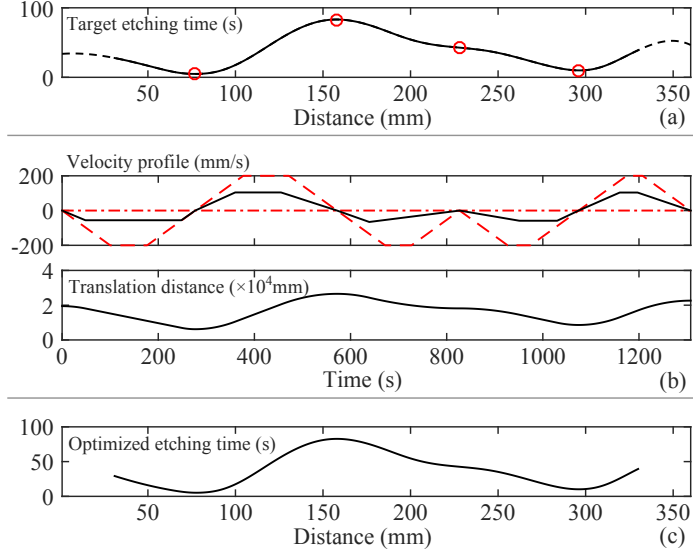


Figure 7: The processing results of an iteration in trajectory optimization, including (a) the target etching time spline, (b) the motion profile, and (c) the optimized etching time curve. First, the target spline is divided into 5 S-curves, then the trapezoidal velocity profile is adjusted within the feasible regions (marked by the red dotted lines), and finally, an optimized etching time curve is obtained by performing the conversions shown in Figure 8.

calculated based on the aforementioned spatio-temporal visualization map.

As shown in Figure 8, there contains two basic steps to calculate the optimized etching times. First, the figuring process is represented by mapping the scanning track of the variable beam spot by normalized removal functions along the scanning distance according to the polled pattern (Figure 8 (a)). Then the etching time curves are obtained by grid-based interpolation of the results of the previous step (Figure 8 (b)), and the optimized etching times are calculated by numerically integrate the interpolated curves along the time axis.

The objective is to minimize the return value of the objective function, i.e., the RMSD of the target etching time profile and the optimized etching time profile, until meeting the requirement or the stop condition. As is shown in Figure 9, the RMSD of the target etching time profile and the optimized etching time profile is 0.2465 s, which is about 0.3% of the peak-to-valley (PV) value of

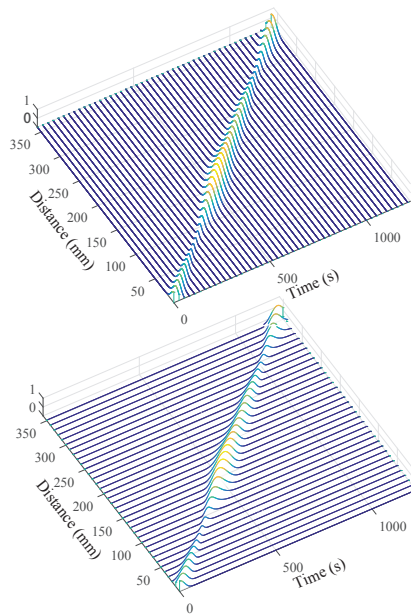


Figure 8: Calculation of optimized etching times. (a) Mapping the scanning track by normalized variable-spot removal functions and (b) obtaining etching time profiles by grid-based interpolation are two basic steps for calculating the optimized etching times, which are integrals of the etching time profiles.

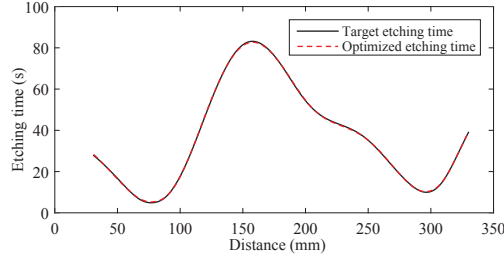


Figure 9: Comparison of the target etching time spline and the optimized etching time curve. The RMSD of the two is about 0.2465 s

the target profile. The optimized result indicates that pattern search is applicable for the trajectory optimization based on S-curve transformation. Moreover, the trajectory optimization using pattern search is a generalized solution for one-dimensional surface figuring with variable-spot tools.

5.2. Two-dimensional figuring with variable-spot ion beam

Figure 10 shows the desired surface map, the programmed surface map, the predicted surface map, and the error map that indicates the differences between the desired map and the predicted map. The programmed surface map is a crossing result obtained by conducting two times of scan path programming. After the scan path programming, we get programmed etching time profiles and then perform trajectory optimization on the programmed etching time profiles one by one, which also can be considered as performing many times of trajectory optimization of one-dimensional figuring. The predicted surface map is the simulated result of variable-spot IBF according to the programmed scan path and the optimized trajectory. The PV value and RMS height of the desired surface map are 180 nm and 38.8 nm. After the figuring in a single iteration, as is summarized in Figure 11, the PV value decreases to about 28 nm and the RMS height becomes about 3.9 nm. It indicates that variable-spot IBF is also competent for the work of precision fabrication of optical surfaces. Note that, in this simulation, the dimensions of these surface map are 300 mm×300 mm and the ion beam width is selected as 36 mm. Under this condition, the RMS

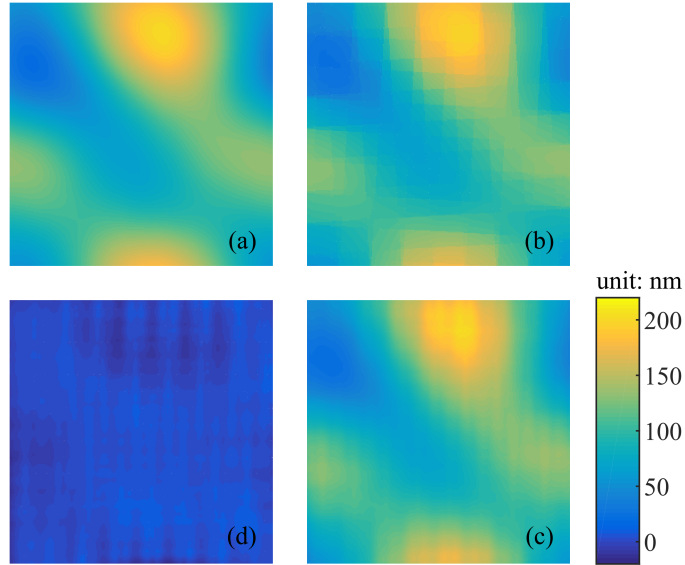


Figure 10: (a) the desired surface map, (b) the programmed surface map, (c) the predicted surface map, and (d) the error map. Note that the programmed surface map is a crossing result and the error map presents etch-depth differences between the desired surface map and the predicted surface map.

height of about 3.9 nm is obtained. If a more smoothing surface is required, we should narrow the ion beam width or increase the number of layers in the scan path programming.

5.2.1. Parameter optimization for scan path programming

By the scan path programming, the two-dimensional optical surface is divided into several groups of belt-like surfaces, which is a process of dimensional reduction that approximately transforms the two-dimensional figuring process into a series of one-dimensional figuring processes. The objective of scan path programming is to search a group of reasonable parameters, including the ion beam width and the number of layers, under which the RMSD of the desired surface map and the programmed surface map would be not greater than the desired value. Figure 12 shows that the RMSD, of the desired surface map and the programmed surface map, decreases as the ion beam width W_{beam} narrows and

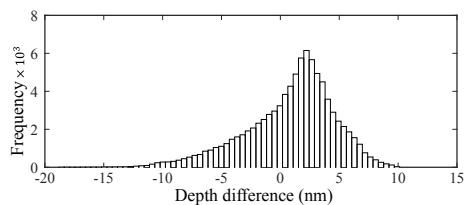


Figure 11: Distribution of etch-depth differences of the desired surface map and the predicted surface map.

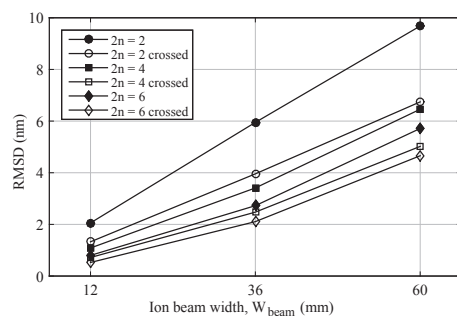


Figure 12: The variation of RMSD with the ion beam width and the number of layers.

the number of layers $2n$ increases. The RMSD crossed is about 4 nm when the ion beam width is 36 mm and the number of layers is 2, which meets our design requirement. Note that the RMSD crossed refers to the RMSD of the target and the crossing result of two times of scan-path programming.

5.2.2. Fine tuning of the maximum etch rate

It has been found that the predicted surface map usually has an overall-shift deviation with the desired surface map. Our strategy for decreasing the overall-shift deviation is finely tuning the maximum etch rate by varying the distance between the ion source and the workpiece. As is shown in Figure 13, the deviation, or rather the RMSD, varies as the maximum etch rates changes. There are many lowlands around the line defined by $x + y = 1.7$. The best point is marked by a cross in Figure 13, where the RMSD is 3.9 nm while the two maximum etch rates are 0.5 nm/s and 1.2 nm/s respectively. Note that there are two times of scan path programming so we can finely tune the maximum etch

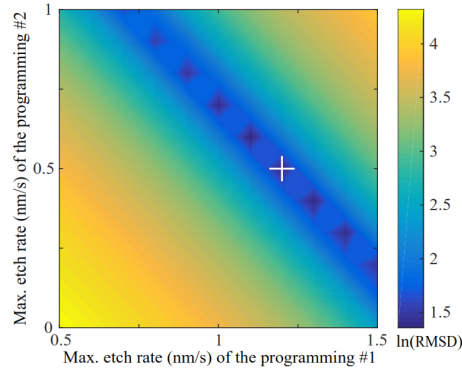


Figure 13: Fine tuning of maximum etch rates. The programming #1 and #2 indicate the first and the second programmed scan path.

rates for the two programmed scan paths respectively. Note also that after the fine tuning, the working condition of the ion source should keep stable during the figuring process.

6. Conclusion

The concepts of figuring with variable spots at constant scanning speed are introduced and the algorithm for variable-spot IBF has also been briefly described. Two simulations are conducted. For the first simulation, its result indicates that the trajectory optimization using pattern search based on S-curve transformation is feasible. And the result of the second simulation verify the feasibility of variable-spot IBF applied to the precision figuring of optical surfaces. The variable-spot IBF is a promising alternative to the conventional IBF. The preliminary analysis suggests that we may also benefit from the combination of the two techniques of IBF. Moreover, the idea of surface figuring or polishing with variable spots is a generalized concept for optical fabrication, from which other advanced techniques of optical fabrication such as plasma jet machining, magnetorheological finishing, and fluid jet polishing can also benefit.

Acknowledgement

The work was partially supported by the National Natural Science Foundation of China under Grant No. 11275201.

References

References

- [1] T. Arnold, G. Bhm, R. Fechner, J. Meister, A. Nickel, F. Frost, T. Hnsel, A. Schindler, Ultra-precision surface finishing by ion beam and plasma jet techniques – status and outlook, *Nucl. Instrum. Meth. A* 616 (23) (2010) 147–156. doi:10.1016/j.nima.2009.11.013.
- [2] P. Shore, P. Morantz, Ultra-precision: enabling our future, *Phil. Trans. R. Soc. A* 370 (1973) (2012) 3993–4014. doi:10.1098/rsta.2011.0638.
- [3] W. Guo, B. Liang, X. Cheng, Y. Zheng, A large ion beam figuring plant used for manufacturing astronomical telescope, *Proc. SPIE* 8416 (2012) 841607–5. doi:10.1117/12.975663.
- [4] M. Ghigo, G. Vecchi, S. Basso, O. Citterio, M. Civitani, E. Mattaini, G. Pareschi, G. Sironi, Ion figuring of large prototype mirror segments for the E-ELT, *Proc. SPIE* 9151 (2014) 91510Q–12. doi:10.1117/12.2056769.
- [5] T. W. Drueding, S. C. Fawcett, S. R. Wilson, T. G. Bifano, Ion beam figuring of small optical components, *Opt. Eng.* 34 (12) (1995) 3565–3571. doi:10.1117/12.215648.
- [6] L. Peverini, I. V. Kozhevnikov, A. Rommeveaux, P. V. Vaerenbergh, L. Claustre, S. Guillet, J. Y. Massonnat, E. Ziegler, J. Susini, Ion beam profiling of aspherical X-ray mirrors, *Nucl. Instrum. Meth. A* 616 (23) (2010) 115–118. doi:10.1016/j.nima.2009.10.169.

- [7] F. Siewert, Metrology, Mirrors and Gratings Advances and Challenges in Synchrotron Optics, *Journal of Physics: Conference Series* 425 (15) (2013) 152001. doi:10.1088/1742-6596/425/15/152001.
- [8] S. G. Alcock, I. Nistea, J. P. Sutter, K. Sawhney, J.-J. Ferm, C. Thellir, L. Peverini, Characterization of a next-generation piezo bimorph X-ray mirror for synchrotron beamlines, *J Synchrotron Radiat* 22 (Pt 1) (2015) 10–15. doi:10.1107/S1600577514020025.
- [9] M. Weiser, Ion beam figuring for lithography optics, *Nucl. Instrum. Meth. B* 267 (89) (2009) 1390–1393. doi:10.1016/j.nimb.2009.01.051.
- [10] T. W. Drueding, T. G. Bifano, S. C. Fawcett, Contouring algorithm for ion figuring, *Precis. Eng.* 17 (1) (1995) 10–21. doi:10.1016/0141-6359(94)00002-H.
- [11] C. Jiao, S. Li, X. Xie, Algorithm for ion beam figuring of low-gradient mirrors, *Appl. Opt.* 48 (21) (2009) 4090. doi:10.1364/AO.48.004090.
- [12] R. A. Jones, W. J. Rupp, Rapid optical fabrication with CCOS, *Proc. SPIE* 1333 (1990) 34–43. doi:10.1117/12.22787.
- [13] A. Schindler, T. Haensel, D. Flamm, W. Frank, G. Boehm, F. Frost, R. Fechner, F. Bigl, B. Rauschenbach, Ion beam and plasma jet etching for optical component fabrication, *Proc. SPIE* 4440 (2001) 217–227. doi:10.1117/12.448043.
- [14] H. R. Kaufman, J. J. Cuomo, J. M. E. Harper, Technology and applications of broadbeam ion sources used in sputtering. Part I. Ion source technology, *J. Vac. Sci. Technol.* 21 (3) (1982) 725–736. doi:10.1116/1.571819.
- [15] W. Liao, Y. Dai, X. Xie, L. Zhou, Mathematical modeling and application of removal functions during deterministic ion beam figuring of optical surfaces Part 1: Mathematical modeling, *Appl. Opt.* 53 (19) (2014) 4266. doi:10.1364/AO.53.004266.

- [16] W. Liao, Y. Dai, X. Xie, L. Zhou, Mathematical modeling and application of removal functions during deterministic ion beam figuring of optical surfaces Part 2: application, *Appl. Opt.* 53 (19) (2014) 4275. doi:10.1364/AO.53.004275.
- [17] D. S. C. Biggs, M. Andrews, Acceleration of iterative image restoration algorithms, *Appl. Opt.* 36 (8) (1997) 1766. doi:10.1364/AO.36.001766.
- [18] L. Wu, K. Qiu, Y. Liu, S. Fu, Algorithms for finely adjusting etch depths to improve the diffraction efficiency uniformity of large-aperture BSG, *J. Opt.* 17 (3) (2015) 035401. doi:10.1088/2040-8978/17/3/035401.
- [19] J. W. Jeon, Y. Y. Ha, A generalized approach for the acceleration and deceleration of industrial robots and CNC machine tools, *IEEE Transactions on Industrial Electronics* 47 (1) (2000) 133–139. doi:10.1109/41.824135.
- [20] P. Jester, C. Menke, K. Urban, B-spline representation of optical surfaces and its accuracy in a ray trace algorithm, *Appl. Opt.* 50 (6) (2011) 822–828. doi:10.1364/AO.50.000822.
- [21] C. Audet, J. Dennis, Analysis of Generalized Pattern Searches, *SIAM J. Optim.* 13 (3) (2002) 889–903. doi:10.1137/S1052623400378742.
- [22] D. Bergstrm, Surface Generation & Analysis - MySimLabs.
URL http://www.mysimlabs.com/surface_generation.html